

Synthesis, Crystal Structure, and Electronic Properties of the Tetragonal  $(RE^I RE^{II})_3SbO_3$  Phases ( $RE^I = La, Ce$ ;  $RE^{II} = Dy, Ho$ )Scott Forbes,<sup>†</sup> Peng Wang,<sup>†</sup> Jinlei Yao,<sup>†,§</sup> Taras Kolodiaznyh,<sup>‡</sup> and Yuriy Mozharivskyy<sup>\*,†</sup><sup>†</sup>Department of Chemistry and Chemical Biology, McMaster University, 1280 Main Street West, Hamilton, Ontario, L8S 4M1, Canada<sup>‡</sup>Institute for Materials Science, 1-1 Namiki, Tsukuba, Ibaraki 305-0044, Japan<sup>§</sup>School of Mathematics and Physics, Suzhou University of Science and Technology, Suzhou 215009, China

## Supporting Information

**ABSTRACT:** In our efforts to tune the charge transport properties of the recently discovered  $RE_3SbO_3$  phases ( $RE$  is a rare earth), we have prepared mixed  $(RE^I RE^{II})_3SbO_3$  phases ( $RE^I = La, Ce$ ;  $RE^{II} = Dy, Ho$ ) via high-temperature reactions at 1550 °C or greater. In contrast to monoclinic  $RE_3SbO_3$ , the new phases adopt the  $P4_2/mmm$  symmetry but have a structural framework similar to that of  $RE_3SbO_3$ . The formation of the tetragonal  $(RE^I RE^{II})_3SbO_3$  phases is driven by the ordering of the large and small  $RE$  atoms on different atomic sites. The  $La_{1.5}Dy_{1.5}SbO_3$ ,  $La_{1.5}Ho_{1.5}SbO_3$ , and  $Ce_{1.5}Ho_{1.5}SbO_3$  samples were subjected to elemental microprobe analysis to verify their compositions and to electrical resistivity measurements to evaluate their thermoelectric potential. The electrical resistivity data indicate the presence of a band gap, which is supported by electronic structure calculations.



and to electrical resistivity measurements to evaluate their thermoelectric potential. The electrical resistivity data indicate the presence of a band gap, which is supported by electronic structure calculations.

## INTRODUCTION

The ever-increasing global demand for natural resources continues to fuel the research on and development of new and efficient ways for energy use. One potential approach is the use of thermoelectric materials for energy recovery from the waste heat, released by internal combustion engines, e.g., in cars and trucks.<sup>1,2</sup> For such applications, thermoelectrics yield many advantages over other forms of energy recovery and production such as compactness, reliability, a lack of moving parts, and a long operational life. These properties have already allowed thermoelectrics to be used in some unique applications, such as power generation on spacecrafts<sup>3</sup> or wristwatches.<sup>4</sup>

The current drawback of thermoelectric materials is their low efficiency, which reaches 5–15% of the Carnot efficiency in the best materials known.<sup>5</sup> As such, thermoelectrics have only seen use in small, niche applications in which compactness and reliability outweigh efficiency. A good thermoelectric material must have a high Seebeck coefficient and electrical conductivity and a low thermal conductivity. Unfortunately, the Seebeck coefficient and electrical conductivity of a material compromise each other and usually cannot both be optimized simultaneously. Likewise, designing a material with good electrical properties and a low thermal conductivity presents a great challenge due to the thermal conductivity provided by charge carriers. Different strategies have been employed to optimize thermoelectric properties. One such method is to prepare phases with electrical properties of a crystalline solid but with thermal conductivities of a glass.<sup>6</sup> Such a material, known as a phonon-glass electron-crystal (PGEC), has been realized in few systems, e.g., in  $Zn_4Sb_3$ <sup>7–9</sup> and  $PbTe$ -based phases.<sup>10,11</sup>

In pursuit of novel PGEC phases, our group has focused on the synthesis of complex rare-earth (RE) antimonide suboxides, such as  $RE_3SbO_3$ ,  $RE_8Sb_{3-6}O_8$ , and  $RE_2SbO_2$ .<sup>12,13</sup> In the case of  $RE_3SbO_3$ , we have combined the electrically conductive, semimetallic  $RESb$  and thermally insulating  $RE_2O_3$  binaries into a single structure, with the goal of conserving the desirable properties of each. The new  $RE_3SbO_3$  phases feature high thermal stability and low thermal conductivity but possess high electrical resistivities, which make them unsuitable for thermoelectric applications. Although the desired properties could not be obtained, we have succeeded in the direct combination of  $RESb$  and  $RE_2O_3$  and the opening of a band gap within the  $RESb$  framework. As such, there is a potential for the  $RE_3SbO_3$  phases if their electrical resistivities can be reduced to a more suitable level, either by elemental substitution or further structural modifications.

Originally, we explored substitution of  $Ce$  for the trivalent  $RE$  in  $RE_3SbO_3$ . However, it was established that  $Ce$  is also trivalent in the prepared  $(CeRE)_3SbO_3$  phases. These new, mixed phases were discovered to have tetragonal symmetry, while the parent  $RE_3SbO_3$  structures were monoclinic. The subsequent experiments revealed that this structural change is possible only through the use of two  $RE$  atoms with a sufficiently large difference in atomic radii, which results in the preferential ordering of large and small rare-earths on different atomic sites. In this paper, we discuss the synthetic conditions, characterization, and electronic structures of the new,

Received: October 18, 2012

Published: January 8, 2013

Table 1. Phase Analysis of the (RE<sup>I</sup>RE<sup>II</sup>)<sub>3</sub>SbO<sub>3</sub> Samples Prepared at 1550 °C

system	RE <sup>I</sup> <sub>2.5</sub> RE <sup>II</sup> <sub>0.5</sub> SbO <sub>3</sub>	RE <sup>I</sup> RE <sup>II</sup> SbO <sub>3</sub>	RE <sup>I</sup> <sub>1.5</sub> RE <sup>II</sup> <sub>1.5</sub> SbO <sub>3</sub>	RE <sup>I</sup> RE <sup>II</sup> <sub>2</sub> SbO <sub>3</sub>	RE <sup>I</sup> <sub>0.5</sub> RE <sup>II</sup> <sub>2.5</sub> SbO <sub>3</sub>
Ce–Gd–Sb–O	-	-	Monoclinic RE <sub>3</sub> SbO <sub>3</sub>	-	-
Ce–Ho–Sb–O	-	-	Tetragonal RE <sub>3</sub> SbO <sub>3</sub>	Monoclinic RE <sub>3</sub> SbO <sub>3</sub> and RE <sub>2</sub> SbO <sub>2</sub>	RE <sub>2</sub> SbO <sub>2</sub>
Ce–Er–Sb–O	-	-	Tetragonal RE <sub>3</sub> SbO <sub>3</sub> and RE <sub>2</sub> SbO <sub>2</sub>	-	-
La–Dy–Sb–O	Monoclinic RE <sub>3</sub> SbO <sub>3</sub>	Monoclinic RE <sub>3</sub> SbO <sub>3</sub>	Tetragonal RE <sub>3</sub> SbO <sub>3</sub>	Tetragonal RE <sub>3</sub> SbO <sub>3</sub>	RE <sub>2</sub> SbO <sub>2</sub>
La–Ho–Sb–O	Monoclinic RE <sub>3</sub> SbO <sub>3</sub>	Monoclinic RE <sub>3</sub> SbO <sub>3</sub>	Tetragonal RE <sub>3</sub> SbO <sub>3</sub>	RE <sub>2</sub> SbO <sub>2</sub>	RE <sub>2</sub> SbO <sub>2</sub>

Table 2. Crystallographic and Refinement Data for the (RE<sup>I</sup>RE<sup>II</sup>)<sub>3</sub>SbO<sub>3</sub> Crystals

	La <sub>1.5</sub> Dy <sub>1.5</sub> SbO <sub>3</sub>	LaDy <sub>2</sub> SbO <sub>3</sub>	La <sub>1.5</sub> Ho <sub>1.5</sub> SbO <sub>3</sub>	Ce <sub>1.5</sub> Ho <sub>1.5</sub> SbO <sub>3</sub>
refined composition	La <sub>1.47(7)</sub> Dy <sub>1.53(7)</sub> SbO <sub>3</sub>	La <sub>0.96(9)</sub> Dy <sub>2.04(9)</sub> SbO <sub>3</sub>	La <sub>1.32(4)</sub> Ho <sub>1.68(4)</sub> SbO <sub>3</sub>	Ce <sub>1.34(9)</sub> Ho <sub>1.66(9)</sub> SbO <sub>3</sub>
space group	<i>P</i> 4 <sub>2</sub> / <i>mmn</i>			
<i>a</i> (Å)	11.947(1)	11.864(2)	11.920(2)	11.880(2)
<i>c</i> (Å)	3.9263(8)	3.8920(8)	3.9057(8)	3.8906(8)
volume (Å <sup>3</sup> )	560.4(1)	547.8(3)	555.0(2)	549.1(2)
<i>Z</i>	4	4	4	4
index ranges	-19 ≤ <i>h</i> ≤ 15 -18 ≤ <i>k</i> ≤ 18 -6 ≤ <i>l</i> ≤ 6	-15 ≤ <i>h</i> ≤ 18 -18 ≤ <i>k</i> ≤ 18 -6 ≤ <i>l</i> ≤ 6	-18 ≤ <i>h</i> ≤ 15 -18 ≤ <i>k</i> ≤ 18 -6 ≤ <i>l</i> ≤ 5	-18 ≤ <i>h</i> ≤ 18 -18 ≤ <i>k</i> ≤ 14 -6 ≤ <i>l</i> ≤ 6
2θ range	6.82–68.96°	6.68–69.01°	6.84–68.70°	6.86–68.96°
total reflections	6684	4159	5522	5304
goodness-of-fit on <i>F</i> <sup>2</sup>	1.187	1.169	1.091	1.029
<i>R</i> indices	<i>R</i> <sub>1</sub> = 0.0378 <i>wR</i> <sub>2</sub> = 0.0760 <i>R</i> <sub>1</sub> (all data) = 0.0532	<i>R</i> <sub>1</sub> = 0.0557 <i>wR</i> <sub>2</sub> = 0.0759 <i>R</i> <sub>1</sub> (all data) = 0.0883	<i>R</i> <sub>1</sub> = 0.0380 <i>wR</i> <sub>2</sub> = 0.0445 <i>R</i> <sub>1</sub> (all data) = 0.0625	<i>R</i> <sub>1</sub> = 0.0519 <i>wR</i> <sub>2</sub> = 0.0617 <i>R</i> <sub>1</sub> (all data) = 0.1019
extinction coefficient	0.0026(2)	0.0012(1)	0.00175(9)	0.00073(6)

Table 3. Atomic Parameters for the (RE<sup>I</sup>RE<sup>II</sup>)<sub>3</sub>SbO<sub>3</sub> Crystals

atom	site	occupancy	<i>x</i>	<i>y</i>	<i>z</i>	<i>U</i> <sub>eq</sub>
La <sub>1.47(7)</sub> Dy <sub>1.53(7)</sub> SbO <sub>3</sub>						
La/Dy1	4 <i>f</i>	0.93/0.07(3)	0.11537(4)	0.11537(4)	0	0.0119(2)
La/Dy2	8 <i>i</i>	0.27/0.73(3)	0.12314(4)	0.65651(5)	0	0.0135(2)
Sb1	4 <i>f</i>	1	0.37828(5)	0.37828(5)	0	0.0124(3)
O1	4 <i>g</i>	1	0.3104(5)	0.6896(5)	0	0.013(2)
O2	8 <i>i</i>	1	0.0660(7)	0.3383(8)	0	0.028(2)
La <sub>0.96(9)</sub> Dy <sub>2.04(9)</sub> SbO <sub>3</sub>						
La/Dy1	4 <i>f</i>	0.75/0.25(4)	0.11601(7)	0.11601(7)	0	0.0135(2)
La/Dy2	8 <i>i</i>	0.11/0.89(4)	0.12298(7)	0.65631(6)	0	0.0116(2)
Sb1	4 <i>f</i>	1	0.37824(8)	0.37824(8)	0	0.0123(4)
O1	4 <i>g</i>	1	0.3110(8)	0.6890(8)	0	0.016(3)
O2	8 <i>i</i>	1	0.0660(9)	0.339(1)	0	0.025(3)
La <sub>1.32(4)</sub> Ho <sub>1.68(4)</sub> SbO <sub>3</sub>						
La/Ho1	4 <i>f</i>	0.92/0.08(2)	0.11539(5)	0.11539(5)	0	0.0119(2)
La/Ho2	8 <i>i</i>	0.20/0.80(2)	0.12319(4)	0.65604(4)	0	0.0139(1)
Sb1	4 <i>f</i>	1	0.37756(5)	0.37756(5)	0	0.0119(2)
O1	4 <i>g</i>	1	0.3100(5)	0.6900(5)	0	0.012(2)
O2	8 <i>i</i>	1	0.0660(6)	0.3394(8)	0	0.029(2)
Ce <sub>1.34(9)</sub> Ho <sub>1.66(9)</sub> SbO <sub>3</sub>						
La/Ce1	4 <i>f</i>	0.88/0.12(4)	0.11523(9)	0.11523(9)	0	0.0130(3)
La/Ce2	8 <i>i</i>	0.23/0.77(4)	0.12372(8)	0.65599(6)	0	0.0130(2)
Sb1	4 <i>f</i>	1	0.37815(9)	0.37815(9)	0	0.0121(4)
O1	4 <i>g</i>	1	0.3122(8)	0.6878(8)	0	0.013(3)
O2	8 <i>i</i>	1	0.067(1)	0.339(1)	0	0.032(3)

tetragonal (RE<sup>I</sup>RE<sup>II</sup>)<sub>3</sub>SbO<sub>3</sub> phases (RE<sup>I</sup> = La, Ce; RE<sup>II</sup> = Dy, Ho).

## EXPERIMENTAL SECTION

**Synthesis.** Samples were made using high-purity RE metals (99.99 wt. %, SmartElements) (RE = La, Ce, Dy, Ho), antimony metal (99.999 wt. %, CERAC Inc.), and RE<sub>2</sub>O<sub>3</sub> and CeO<sub>2</sub> powder (99.999

wt. %, Rhône-Poulenc). To avoid the volatility of elemental antimony and its reactivity with tantalum at elevated temperatures, the corresponding RESb binaries were first prepared. The RESb binaries were prepared by mixing RE filings with ground antimony powder in equimolar amounts within a glovebox filled with argon. These mixtures were then pressed into pellets of 1–2 g and sealed below 10<sup>-5</sup> Torr in silica tubes. Samples were annealed in box furnaces at a temperature of 600 °C for 12 h and then at 850 °C for 48 h to complete the reaction.

Table 4. Compositions of the Tetragonal (RE<sup>I</sup>RE<sup>II</sup>)<sub>3</sub>SbO<sub>3</sub> Phases Based on the EPMA and the X-ray Single-Crystal Analyses<sup>a</sup>

loading Composition	EPMA	X-ray
La <sub>1.5</sub> Dy <sub>1.5</sub> SbO <sub>3</sub>	La <sub>1.45(7)</sub> Dy <sub>1.53(7)</sub> Sb <sub>1.00(8)</sub> O <sub>6.42(5)</sub>	La <sub>1.47(7)</sub> Dy <sub>1.53(7)</sub> SbO <sub>3</sub>
La <sub>1.5</sub> Ho <sub>1.5</sub> SbO <sub>3</sub>	La <sub>1.54(6)</sub> Ho <sub>1.52(6)</sub> Sb <sub>1.00(8)</sub> O <sub>5.98(5)</sub>	La <sub>1.32(4)</sub> Ho <sub>1.68(4)</sub> SbO <sub>3</sub>
Ce <sub>1.5</sub> Ho <sub>1.5</sub> SbO <sub>3</sub>	Ce <sub>1.54(6)</sub> Ho <sub>1.47(6)</sub> Sb <sub>1.00(7)</sub> O <sub>5.13(5)</sub>	Ce <sub>1.34(9)</sub> Ho <sub>1.66(9)</sub> SbO <sub>3</sub>

<sup>a</sup>The EPMA results were normalized to one Sb atom.

Upon quenching in air, black pellets of RESb were obtained. X-ray powder diffraction was performed on all samples to confirm their purity.

Samples of RE<sup>I</sup><sub>1.5</sub>RE<sup>II</sup><sub>1.5</sub>SbO<sub>3</sub> were prepared by mixing the RESb binaries and RE<sub>2</sub>O<sub>3</sub> for each of the respective REs present in a 1:1:1:1 molar ratio. The uneven RE<sup>I</sup>:RE<sup>II</sup> ratio (RE<sup>I</sup>RE<sup>II</sup>)<sub>3</sub>SbO<sub>3</sub> samples were prepared by mixing the respective RESb and RE<sub>2</sub>O<sub>3</sub> binaries to produce the desired stoichiometry. The (CeRE<sup>II</sup>)<sub>3</sub>SbO<sub>3</sub> samples were prepared by mixing filed RE metal, the RESb binaries, and CeO<sub>2</sub> in the desired molar ratio. The respective mixtures were pressed into pellets of 1 g and placed inside tantalum ampules which were then sealed by arc-melting under an argon atmosphere. High-temperature reaction conditions were accomplished through the use of an induction furnace. The tantalum ampules containing samples were placed inside a molybdenum suscepter which was heated in the radio frequency furnace under dynamic vacuum below 10<sup>-5</sup> Torr. An optical pyrometer was used to monitor the temperature of the reaction. All samples were heated at 1550 °C for 10 h to ensure a complete reaction. Samples were allowed to cool to room temperature inside the furnace under vacuum over a period of 1 h. The obtained products were black, molten, crystalline, and stable in air. According to X-ray powder diffraction analysis, samples exposed to air for several weeks showed no signs of decomposition. A list of all samples prepared is presented in Table 1.

**X-ray Single Crystal Diffraction.** Single crystals picked up from the samples were analyzed on a STOE IPDSII diffractometer using Mo K $\alpha$  radiation in the whole reciprocal sphere. A numerical absorption correction was based on the crystal shape originally determined by optical face indexing but was later optimized against equivalent reflections using the STOE X-Shape software.<sup>14</sup> Crystal structures were determined and solved using the SHELX software.<sup>15</sup> All structures studied adopt the P4<sub>2</sub>/mmm space group. The lattice parameters of structures were observed to expand with larger RE atoms. During refinement, the RE atoms were permitted to mix on the RE1 and RE2 sites, yielding mixed occupancy on both sites for all structures. While the occupancies of Dy and Ho on the RE1 site in La<sub>1.47(7)</sub>Dy<sub>1.53(7)</sub>SbO<sub>3</sub> and Ce<sub>1.34(9)</sub>Ho<sub>1.66(9)</sub>SbO<sub>3</sub> are within three standard deviations from zero, the Hamilton test<sup>16</sup> indicated that their presence on this site can be accepted with a higher than 0.995 confidence level. A summary of the refinement results is presented in Tables 2 and 3. Further information on the crystal structures of all compounds presented, including the monoclinic Dy<sub>3</sub>SbO<sub>3</sub> structure collected for this work, can be obtained from the Fachinformationszentrum Karlsruhe, 76344 Eggenstein-Leopoldshafen, Germany (fax (49) 7247-808-666; e-mail crysdata@fiz.karlsruhe.de), by quoting the CSD depository numbers 425138 for Ce<sub>1.5</sub>Ho<sub>1.5</sub>SbO<sub>3</sub>, 425139 for La<sub>1.5</sub>Dy<sub>1.5</sub>SbO<sub>3</sub>, 425140 for La<sub>1.5</sub>Ho<sub>1.5</sub>SbO<sub>3</sub>, 425141 for Dy<sub>3</sub>SbO<sub>3</sub>, and 425150 for LaDy<sub>2</sub>SbO<sub>3</sub> samples.

**X-ray Powder Diffraction.** All samples studied were analyzed by X-ray powder diffraction using a PANalytical X'Pert Pro diffractometer with the Cu K $\alpha$  radiation and an X'Celerator detector. This was done to determine reaction progression, sample purity, and lattice constants. Samples were ground in 20–50 mg amounts in a mortar and pestle until a fine powder was obtained. The obtained powder was distributed evenly on disks manufactured from single crystals of silicon which were coated with a thin film of Vaseline. Diffraction data were collected in the 20–70° 2 $\theta$  range for all samples. The Rietveld refinement method (Rietica program<sup>17</sup>) was employed to determine sample purity and lattice constants. The structural parameters obtained from the single-crystal refinements were used as starting models.

**Coordination Polyhedra Analysis.** Coordination polyhedra of the new tetragonal (RE<sup>I</sup>RE<sup>II</sup>)<sub>3</sub>SbO<sub>3</sub> structures, the previously studied monoclinic Ho<sub>3</sub>SbO<sub>3</sub> phase,<sup>12</sup> and the monoclinic Dy<sub>3</sub>SbO<sub>3</sub> phase prepared for this work were analyzed with the Dido95 program.<sup>18</sup> For this purpose, we have calculated the volumes of the RE sites, which are represented by the volumes of the Wigner–Seitz polyhedra. Atomic positions determined from the X-ray single-crystal solutions were used for calculations.

**Microprobe Measurements.** The quantitative elemental analysis of the selected samples was performed employing the electron probe microanalysis (EPMA) through a wavelength dispersive (WDS) X-ray spectroscopy (model JXA-8500F, JEOL, Tokyo, Japan). LaB<sub>6</sub>, CeB<sub>6</sub>, Al<sub>2</sub>O<sub>3</sub>, Ho<sub>3</sub>Sb<sub>3</sub>, and DySb were used as standards to determine the concentrations of La, Ce, Ho, Sb, Dy, and O in the title compounds. The EPMA was performed on polished surface samples by averaging the data taken from 5 to 10 locations of selected grains. Only the RE<sup>I</sup><sub>1.5</sub>RE<sup>II</sup><sub>1.5</sub>SbO<sub>3</sub> samples were analyzed for measurement as these samples yielded the best purities.

**Electrical Resistivity Measurements.** Samples of La<sub>1.5</sub>Dy<sub>1.5</sub>SbO<sub>3</sub>, La<sub>1.5</sub>Ho<sub>1.5</sub>SbO<sub>3</sub>, and Ce<sub>1.5</sub>Ho<sub>1.5</sub>SbO<sub>3</sub> were ground and pressed into pellets with a tungsten carbide press die in a glovebox under argon atmosphere. Only the RE<sup>I</sup><sub>1.5</sub>RE<sup>II</sup><sub>1.5</sub>SbO<sub>3</sub> set of samples was chosen for measurement as the highest purities were obtained for this stoichiometry. Samples were then sealed in evacuated silica tubes and annealed at 1000 °C for 24 h to ensure rigidity. X-ray powder diffraction revealed no decomposition or generation of impurities.

The electrical resistivity was measured in the 2–400 K range on rectangular-shaped samples with a four-probe technique using a press contact assembly produced by Wimush Science & Technology and on a PPMS instrument (Quantum Design, USA). During the measurements, the samples were heated with a speed of 1 K/min to allow thermal equilibration with a cryostat.

**Electronic Band Structure Calculations.** The band structures of the tetragonal fully ordered RE<sup>I</sup>RE<sup>II</sup><sub>2</sub>SbO<sub>3</sub> phases (LaDy<sub>2</sub>SbO<sub>3</sub>, LaHo<sub>2</sub>SbO<sub>3</sub>, and CeHo<sub>2</sub>SbO<sub>3</sub>) were calculated using the tight-binding, linear-muffin tin orbital method<sup>19</sup> with the atomic sphere approximation (TB-LMTO-ASA) as implemented in the Stuttgart program.<sup>20</sup> The experimental lattice and atomic parameters obtained from the X-ray single-crystal refinements of the LaDy<sub>2</sub>SbO<sub>3</sub>, La<sub>1.5</sub>Ho<sub>1.5</sub>SbO<sub>3</sub>, and Ce<sub>1.5</sub>Ho<sub>1.5</sub>SbO<sub>3</sub> samples were used for calculations. Since the atomic mixing cannot be treated during calculations, the RE1 and RE2 sites in each structure were assumed to be fully occupied by the larger and smaller RE, respectively. All 4f electrons were considered as core electrons. Exchange and correlation were treated by the local density approximation (LDA).<sup>21</sup> A scalar relativistic approximation<sup>22</sup> was employed to account for all relativistic effects except spin–orbit coupling. Overlapping Wigner–Seitz cells were constructed with radii determined by requiring the overlapping potential to be the best approximation to the full potential, according to the atomic sphere approximation (ASA). Automatic sphere generation<sup>23</sup> was performed to construct empty spheres to be included in the unit cell to satisfy the overlap criteria of the TB-LMTO-ASA model.

## RESULTS AND DISCUSSION

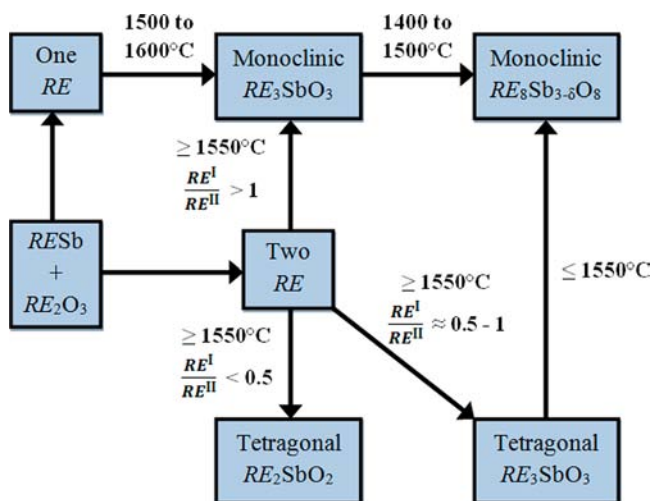
**Composition and Formation of (RE<sup>I</sup>RE<sup>II</sup>)<sub>3</sub>SbO<sub>3</sub>.** The X-ray single-crystal refinements of the La<sub>1.5</sub>Dy<sub>1.5</sub>SbO<sub>3</sub> and Ce<sub>1.5</sub>Ho<sub>1.5</sub>SbO<sub>3</sub> crystals yielded compositions (Table 3) that are within 1 and 2 standard deviations from the loading compositions, respectively. Refinement of the La<sub>1.5</sub>Ho<sub>1.5</sub>SbO<sub>3</sub> crystal yielded the La<sub>1.32(4)</sub>Ho<sub>1.68(4)</sub>SbO<sub>3</sub> composition that is

statistically different from the loading one. In some cases, X-ray single-crystal results may not represent the actual composition, particularly when an atomic mixing is present and the difference between the atomic scattering factors is not large. To establish true compositions (and verify refinement results), electron probe microanalyses (EPMA) were performed on three  $RE^I_{1.5}RE^{II}_{1.5}SbO_3$  samples (Table 4). Upon inspecting Table 4, it is readily apparent that the equimolar loading ratios of the RE atoms are preserved across all samples within one standard deviation. An excess of oxygen is observed, but this can be attributed to the surface oxidation during polishing. On the basis of the EPMA results, we can conclude that  $(RE^I RE^{II})_3SbO_3$  phases maintain the same rare-earth compositions that are used in their formation.

Samples with loading compositions containing different ratios of  $RE^I$  to  $RE^{II}$  were also prepared using reaction conditions similar to the samples with the equimolar ratios. The synthesis of  $LaDy_2SbO_3$  ( $RE^I = La$  and  $RE^{II} = Dy$ ) was confirmed to produce the tetragonal  $RE_3SbO_3$  structure, but with a smaller unit cell when compared to  $La_{1.5}Dy_{1.5}SbO_3$ . Reactions of the  $RE^I_2RE^{II}SbO_3$  and  $RE^I_{2.5}RE^{II}_{0.5}SbO_3$  phases yielded only the monoclinic  $RE_3SbO_3$  phases; these samples were not analyzed further. In contrast, the  $RE^I RE^{II}_2SbO_3$  and  $RE^I_{0.5}RE^{II}_{2.5}SbO_3$  samples, excluding  $LaDy_2SbO_3$ , were shown to produce the  $RE_2SbO_2$  phase. The rationalization for forming each phase at different  $RE^I$  to  $RE^{II}$  ratios will be discussed later.

The tetragonal  $(RE^I RE^{II})_3SbO_3$  phases can be obtained only at reaction temperatures of 1550 °C and greater; at temperatures less than 1500 °C, either the corresponding  $RE_8Sb_{3-\delta}O_8$  or  $RE_2SbO_2$  phase is formed depending on the  $RE^I$  and  $RE^{II}$  used and their ratios. When only one type of RE is used, the resulting phase is always either the monoclinic  $RE_3SbO_3$  phase or the monoclinic  $RE_8Sb_{3-\delta}O_8$  phase at temperatures of at least 1550 °C. The formation conditions for  $(RE^I RE^{II})_3SbO_3$  are summarized in Scheme 1. It is worth

**Scheme 1. Procedures of Formation of the Phases Studied in the RE–Sb–O System**



mentioning that prolonged heat treatments below 1550 °C will irreversibly convert the tetragonal  $(RE^I RE^{II})_3SbO_3$  phase into the corresponding monoclinic  $RE_3SbO_3$  and  $RE_8Sb_{3-\delta}O_8$  phases, with mixing on all RE sites. The tetragonal phase can be prepared for samples containing two REs of significantly different sizes, which limits the possible combinations. On the

basis of the crystal radii of the rare-earth atoms<sup>24</sup> used, the lowest large-to-small ratio of rare-earth radii shown to produce the phase is 1.23, accomplished with  $Ce_{1.5}Ho_{1.5}SbO_3$ . Furthermore, an attempt to prepare the tetragonal  $Ce_{1.5}Gd_{1.5}SbO_3$  analogue was unsuccessful. Considering the crystal radii ratio of Ce to Gd is 1.19, it appears the minimum ratio required may lie between these two values. The reasons for the formation of the tetragonal structure as opposed to the monoclinic phase for the mixed  $(RE^I RE^{II})_3SbO_3$  phases are discussed below.

**Structures and Preferential Site Occupancy.** The  $(RE^I RE^{II})_3SbO_3$  phases of interest adopt a novel crystal structure with the  $P4_2/mnm$  space group. The structure is defined by a REO framework composed of edge-sharing  $RE_4O$  tetrahedra. Three  $RE_4O$  tetrahedra are fused via edge-sharing to form  $RE_8O_3$  units referred to as building blocks. Within the  $ab$  plane, these blocks connect to each other via corners to build 2D slabs (Figure 1). In turn, the slabs stack along the  $c$

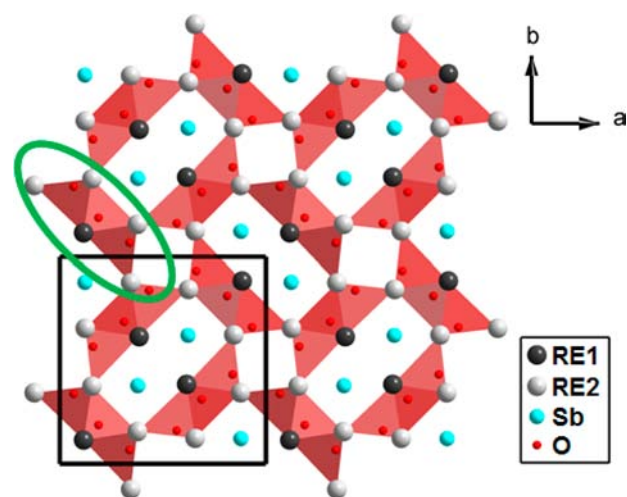


**Figure 1. Tetragonal  $(RE^I RE^{II})_3SbO_3$  structure and its building block type composed of  $RE_4O$  tetrahedra.**

direction via edge-sharing to form the 3D REO framework. Additionally, square and rectangular channels along the  $c$  direction are created by this arrangement. The rectangular voids are occupied by two Sb atoms, and the square voids are left unoccupied. The Sb–Sb separations are too large to support dimer formation, as the shortest distance between these atoms is  $\sim 4$  Å.<sup>25</sup> An interesting aspect of the  $(RE^I RE^{II})_3SbO_3$  phases is the position and displacement parameters for the O2 atoms located in the tetrahedral voids on each side of a  $RE_8O_3$  building block. The O2 atoms are displaced from the center of RE tetrahedra toward the center of a terminal triangular face. The large displacement parameters of the O2 atoms are also directed toward the centers of these terminal triangular faces. Such a feature is likely due to anion–anion repulsion between O1 and O2 atoms in the same building block, which pushes the outside O2 atoms further away from their ideal position at the center of each  $RE_4O$  unit, and as a result yields high displacement parameters.

It is useful to view these phases in a simplified form as  $RE_3SbO_3$ , which has the same composition as the previously studied monoclinic  $RE_3SbO_3$  phases.<sup>12</sup> Both structures include REO frameworks which define the overall structure and empty channels occupied by Sb atoms. Aside from their differences in

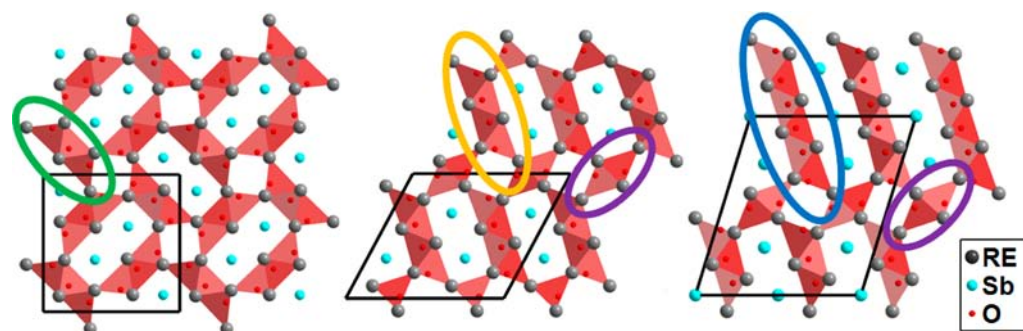


**Figure 2.** Comparison of the tetragonal  $(RE^I RE^{II})_3SbO_3$  (left), monoclinic  $RE_3SbO_3$  (middle), and monoclinic  $RE_8Sb_{3-\delta}O_8$  (right) phases. Different building block types are highlighted with different colors.

symmetry, the two  $RE_3SbO_3$  phases can be easily distinguished by their building block types and arrangements (Figure 2). The previously studied monoclinic  $RE_3SbO_3$  phase contains two distinct building blocks, A and B, which are four and two tetrahedral  $RE_4O$  units long, respectively. In contrast, the newly discovered tetragonal  $(RE^I RE^{II})_3SbO_3$  phase contains only one type of building block, which is three  $RE_4O$  tetrahedra long in all directions, accounting for its higher symmetry. Both structures also have large displacement parameters for the oxygen atoms located at the ends of the building blocks. This unusual feature appears to be preserved among the rare-earth antimonide oxide series, as the  $RE_8Sb_{3-\delta}O_8$  phase (Figure 2) also has terminal O atoms with large displacement parameters.

The  $(RE^I RE^{II})_3SbO_3$  structure contains two RE sites which both have mixed occupancy. The RE1 site (4f) located in the center of each building block is preferentially (>75%) occupied by larger RE atoms (Table 3). Conversely, the RE2 position (8i), which makes the outside corners of the  $RE_8O_3$  building blocks, strongly (>73%) prefers the smaller RE atoms. The site preference was analyzed based on the polyhedra volume (Figure 3) and electronegativity of the  $RE^I$  and  $RE^{II}$  atoms. In

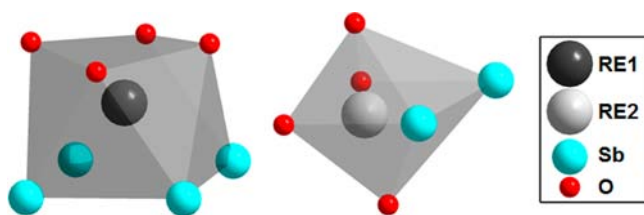


**Figure 3.** Coordination polyhedra of the RE1 site (left) and the RE2 site (right) in the tetragonal  $(RE^I RE^{II})_3SbO_3$  phases.

$(RE^I RE^{II})_3SbO_3$ , RE1 atoms occupy distorted square antiprisms with one face consisting of oxygen atoms and another face consisting of Sb atoms, while RE2 atoms sit in distorted octahedra made of four oxygen atoms and two antimony atoms. The site volumes, calculated with the Dido95 program,<sup>18</sup> are given in Table 5. The RE1 site volume is almost 25% larger than the RE2 site volume, and thus this site should be preferentially occupied by larger RE atoms. Also, the electronegativity difference favors such an RE distribution; the larger RE atoms are more electropositive and as such they can support anion-rich environments (RE1 site) better than the smaller and more electronegative RE atoms.

The presence of the RE1 and RE2 sites with largely different volumes within the tetragonal  $(RE^I RE^{II})_3SbO_3$  structures appears to be the reason for the existence of these mixed

**Table 5.** Coordination Polyhedra Volumes of the Largest and Smallest Sites in the Tetragonal  $(RE^I RE^{II})_3SbO_3$  and Monoclinic  $RE_3SbO_3$  Phases

phase	smallest RE site volume <sup>a</sup>	largest RE site volume <sup>a</sup>	relative size difference
Tetragonal Phases			
$La_{1.47(7)}Dy_{1.53(7)}SbO_3$	17.02(3) Å <sup>3</sup>	21.20(4) Å <sup>3</sup>	24.6(3)%
$La_{1.32(4)}Ho_{1.68(4)}SbO_3$	16.76(3) Å <sup>3</sup>	21.15(4) Å <sup>3</sup>	26.2(3)%
$Ce_{1.34(9)}Ho_{1.66(9)}SbO_3$	16.73(3) Å <sup>3</sup>	20.67(4) Å <sup>3</sup>	23.5(3)%
$La_{0.96(9)}Dy_{2.04(9)}SbO_3$	16.62(3) Å <sup>3</sup>	20.72(4) Å <sup>3</sup>	24.7(3)%
Monoclinic Phases			
$Dy_3SbO_3$	15.98(3) Å <sup>3</sup>	18.44(4) Å <sup>3</sup>	15.4(3)%
$Ho_3SbO_3$	15.79(3) Å <sup>3</sup>	18.28(4) Å <sup>3</sup>	15.8(3)%

<sup>a</sup>In tetragonal  $(RE^I RE^{II})_3SbO_3$ , the largest RE site is RE1, and the smallest is RE2.

phases. Table 5 gives the site volumes for the monoclinic  $Dy_3SbO_3$  and  $Ho_3SbO_3$  phases in addition to those for the mixed phases. It is evident that in the monoclinic  $RE_3SbO_3$  phase the RE sites are quite similar in volume to one another, as the maximum relative volume difference of the RE sites in the monoclinic  $RE_3SbO_3$  structures is only about 15%, yet this difference is about 10% higher in each of the tetragonal  $(RE^I RE^{II})_3SbO_3$  structures. Thus, it is easy for any RE atom to occupy the RE sites evenly in the monoclinic  $RE_3SbO_3$  phase. However, in the tetragonal  $(RE^I RE^{II})_3SbO_3$  phase, the two RE sites are significantly different in size, and if only one RE atom is used, it is not possible for simultaneous occupation of both sites due to their large volume difference. As a result, the structure cannot be formed. Through the usage of two different REs with significantly different sizes, a preference of one RE to occupy one site over another is introduced, and this supports the novel tetragonal REO framework. However, a full separation of the  $RE^I$  and  $RE^{II}$  atoms on the two sites is not achieved.

The tetragonal structure can be preserved with the  $RE^I RE^{II}_2SbO_3$  stoichiometry, for at least  $LaDy_2SbO_3$ , as the larger RE1 site can easily accommodate more of the small RE with some additional occupation on the RE2 site. The net result is no change in the coordination polyhedra volume between the  $La_{1.5}Dy_{1.5}SbO_3$  and  $LaDy_2SbO_3$  structures (24.6(3)% vs 24.7(3)%). It is not known why  $LaDy_2SbO_3$  forms the tetragonal  $(RE^I RE^{II})_3SbO_3$  phase while the  $LaHo_2SbO_3$  and  $CeHo_2SbO_3$  samples do not. However, based on the occupations of the RE sites in the  $LaDy_2SbO_3$  crystal solution, it is likely that the  $RE^I RE^{II}_2SbO_3$  stoichiometry is near the limit of compositions that can form the tetragonal  $(RE^I RE^{II})_3SbO_3$  phase, and perhaps a small change in site

occupations for the  $\text{LaHo}_2\text{SbO}_3$  and  $\text{CeHo}_2\text{SbO}_3$  samples results in the destruction of the desired phase.

The  $\text{RE}^{\text{I}}\text{RE}^{\text{II}}\text{SbO}_3$  and  $\text{RE}_{1.5}^{\text{I}}\text{RE}_{0.5}^{\text{II}}\text{SbO}_3$  phases studied were shown to not preserve the tetragonal  $(\text{RE}^{\text{I}}\text{RE}^{\text{II}})_3\text{SbO}_3$  structure. This is because the larger RE1 site is already nearly fully occupied by the large RE (~90% in each structure), and as a result, the smaller RE2 site must be occupied instead. This in turn destroys the size difference between the two sites and leads to destabilization of the phase. Finally, the  $\text{RE}^{\text{I}}\text{RE}^{\text{II}}_2\text{SbO}_3$  and  $\text{RE}_{0.5}^{\text{I}}\text{RE}_{2.5}^{\text{II}}\text{SbO}_3$  samples (excluding  $\text{LaDy}_2\text{SbO}_3$ ) were shown to form the  $\text{RE}_2\text{SbO}_2$  phase. This may occur since the high  $\text{RE}^{\text{II}}$  content cannot maintain the large size difference in the RE sites for the tetragonal structure, and as pointed out in previous literature,<sup>12</sup> the monoclinic  $\text{RE}_3\text{SbO}_3$  phases require higher temperatures to form for the late rare earths. Since the  $\text{Ce}_{0.5}\text{Ho}_{2.5}\text{SbO}_3$  and  $\text{La}_{0.5}\text{Ho}_{2.5}\text{SbO}_3$  samples mostly consist of holmium, they can be viewed as  $\text{Ho}_3\text{SbO}_3$ , and thus temperatures of at least 1600 °C will be required to form monoclinic  $\text{RE}_3\text{SbO}_3$ . Since neither the monoclinic nor the tetragonal  $\text{RE}_3\text{SbO}_3$  phase can form, the  $\text{RE}_2\text{SbO}_2$  phase becomes the preferred outcome for the  $\text{RE}_{0.5}^{\text{I}}\text{RE}_{2.5}^{\text{II}}\text{SbO}_3$  samples.

**Electrical Resistivity and Electronic Structure.** Assuming that La, Dy, and Ho atoms are in +3 oxidation states and that Sb and O atoms act as isolated anions, the electronic formulas of  $(\text{RE}^{\text{I}}\text{RE}^{\text{II}})_3\text{SbO}_3$  can be written as  $(\text{RE}^{\text{I}(3+)}\text{RE}^{\text{II}(3+)})_3(\text{Sb}^{3-})(\text{O}^{2-})_3$ . It is readily apparent that the  $\text{La}_{1.5}\text{Dy}_{1.5}\text{SbO}_3$  and  $\text{La}_{1.5}\text{Ho}_{1.5}\text{SbO}_3$  structures are charge balanced and may be semiconducting. However, the  $\text{Ce}_{1.5}\text{Ho}_{1.5}\text{SbO}_3$  structure is somewhat ambiguous;  $\text{CeO}_2$  was used as a reactant which contains cerium atoms in the +4 oxidation state. While it is true that Ho metal is oxidized in the reaction with  $\text{CeO}_2$  to make  $\text{Ce}_{1.5}\text{Ho}_{1.5}\text{SbO}_3$ , cerium in the mixed valence state could still be present in the structure, giving the sample metallic behavior. This ambiguity was later resolved through electrical conductivity measurements.

The  $\text{Ce}_{1.5}\text{Ho}_{1.5}\text{SbO}_3$ ,  $\text{La}_{1.5}\text{Dy}_{1.5}\text{SbO}_3$ , and  $\text{La}_{1.5}\text{Ho}_{1.5}\text{SbO}_3$  samples show an Arrhenius-type exponential decrease in electrical resistivity with increasing temperature, which is indicative of semiconducting behavior and in support of the charge-balanced formulas. This also suggests that  $\text{Ce}_{1.5}\text{Ho}_{1.5}\text{SbO}_3$  contains only  $\text{Ce}^{3+}$  and no  $\text{Ce}^{4+}$ , as this would lead to extra carrier electrons and metallic-type behavior in the sample. The activation energies were calculated based on Arrhenius-type behavior for a nondegenerate semiconductor with both electrons and holes as charge carriers. The room-temperature electrical conductivities and activation energies are presented in Table 6. The electrical resistivities for all samples measured in this work are shown in Figure 4.

The La-containing samples displayed fairly similar electrical resistivities above 50 K, which is expected considering the similar chemistry between Dy and Ho. However, below 50 K, the resistivity of  $\text{La}_{1.5}\text{Dy}_{1.5}\text{SbO}_3$  was found to increase. Such

**Table 6. Room-Temperature Electrical Resistivities and Activation Energies of the  $\text{La}_{1.5}\text{Dy}_{1.5}\text{SbO}_3$ ,  $\text{La}_{1.5}\text{Ho}_{1.5}\text{SbO}_3$ , and  $\text{Ce}_{1.5}\text{Ho}_{1.5}\text{SbO}_3$  Samples**

sample	electrical resistivity ( $\Omega$ cm)	activation energy (eV)
$\text{La}_{1.5}\text{Dy}_{1.5}\text{SbO}_3$	1.05	0.11
$\text{La}_{1.5}\text{Ho}_{1.5}\text{SbO}_3$	1.05	0.093
$\text{Ce}_{1.5}\text{Ho}_{1.5}\text{SbO}_3$	0.223	0.044

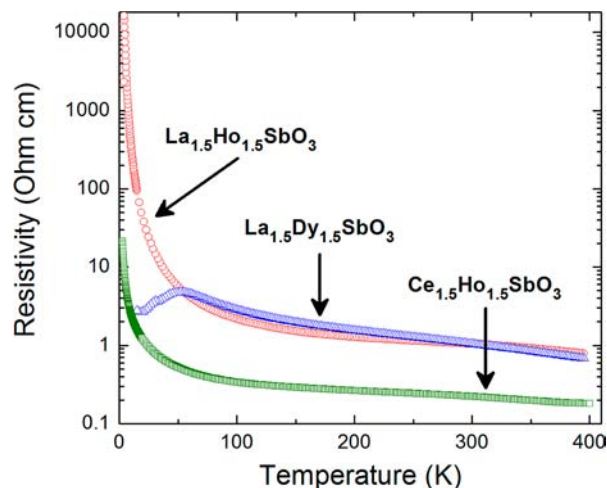


**Figure 4.** Electrical resistivities of the  $\text{Ce}_{1.5}\text{Ho}_{1.5}\text{SbO}_3$ ,  $\text{La}_{1.5}\text{Dy}_{1.5}\text{SbO}_3$ , and  $\text{La}_{1.5}\text{Ho}_{1.5}\text{SbO}_3$  samples.

behavior may be due to (1) a highly conductive impurity, which dominates the electrical transport properties at low temperature, (2) minor deficiencies, which would change conductivity from semiconductor-like to metal-like, or (3) a semiconductor-to-metal transition, which may occur as the result of the  $\text{Sb}_2^{4-}$  dimer formation, accompanied by the release of conduction electrons. To date, we have not resolved the origin of this unexpected behavior; we leave this work for future investigation.

Upon inspection, it is also observed that all samples measured have electrical resistivities of  $\sim 0.1$ – $1 \Omega$  cm or greater at all temperatures measured, which are roughly 2 orders of magnitude greater than the resistivities of benchmark thermoelectric materials.<sup>26</sup> Additionally, these samples generally have electrical resistivities roughly equal to the monoclinic  $\text{RE}_3\text{SbO}_3$  and  $\text{RE}_8\text{Sb}_{3-\delta}\text{O}_8$  phases. Taking these facts into consideration, these new phases do not pose any foreseeable use for thermoelectric applications in their current states.

Semiconducting properties of the  $(\text{RE}^{\text{I}}\text{RE}^{\text{II}})_3\text{SbO}_3$  phases were verified through the electronic structure calculations on the fully ordered  $\text{RE}^{\text{I}}\text{RE}^{\text{II}}_2\text{SbO}_3$  structures. The calculated densities of states, DOS, of  $\text{LaDy}_2\text{SbO}_3$ ,  $\text{LaHo}_2\text{SbO}_3$ , and  $\text{CeHo}_2\text{SbO}_3$  are very similar. The electronic structure of  $\text{LaDy}_2\text{SbO}_3$  is presented in Figure 5, and those of  $\text{LaHo}_2\text{SbO}_3$  and  $\text{CeHo}_2\text{SbO}_3$  can be found in the Supporting Information. An important feature of the DOS is the presence of a small band gap of about 0.3 eV, which separates the conduction band from the valence band. In agreement with the  $(\text{RE}^{(3+)\text{I}}\text{RE}^{(3+)\text{II}})_3(\text{Sb}^{3-})(\text{O}^{2-})_3$  formula, the conduction band is primarily composed of the RE d states, and the valence band is dominated by the Sb p states, as the O p states are much lower in energy.

## CONCLUSIONS

The mixed tetragonal  $(\text{RE}^{\text{I}}\text{RE}^{\text{II}})_3\text{SbO}_3$  compounds are small-band-gap semiconductors similar to the previously studied monoclinic  $\text{RE}_3\text{SbO}_3$  and  $\text{RE}_8\text{Sb}_{3-\delta}\text{O}_8$  phases. On the basis of the electronic structure calculations, combining semimetallic RESb with corresponding  $\text{RE}_2\text{O}_3$  opens a band gap between the valence band dominated by the Sb states and the conduction band composed of the RE states. The semiconducting properties of the  $\text{Ce}_{1.5}\text{Ho}_{1.5}\text{SbO}_3$  phase support the +3

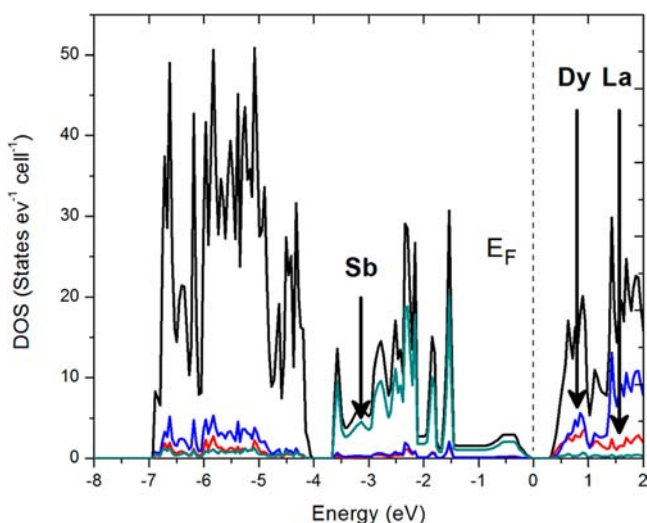


Figure 5. Total and partial densities of state for  $\text{LaDy}_2\text{SbO}_3$ .

oxidation state for Ce, as a mixed valence state would yield a metallic behavior. The  $\text{RE}^{\text{I}}_{1.5}\text{RE}^{\text{II}}_{1.5}\text{SbO}_3$  samples display room-temperature electrical resistivities in the 0.1–1  $\Omega$  cm range, similar to the  $\text{RE}_3\text{SbO}_3$  and  $\text{RE}_8\text{Sb}_{3-8}\text{O}_8$  phases, which is too large for thermoelectric applications.

The tetragonal  $(\text{RE}^{\text{I}}\text{RE}^{\text{II}})_3\text{SbO}_3$  phases are obtained at temperatures above 1550  $^\circ\text{C}$  and only when two RE atoms with highly different atomic radii are used. While the  $\text{RE}^{\text{I}}$  and  $\text{RE}^{\text{II}}$  atoms are distributed on both RE sites, there is a pronounced site preference; larger atoms tend to occupy the larger site (4f) and smaller atoms occupy the smaller site (8i). Compared to the analogous monoclinic  $\text{RE}_3\text{SbO}_3$  structures, the RE site volumes differ significantly in the tetragonal  $(\text{RE}^{\text{I}}\text{RE}^{\text{II}})_3\text{SbO}_3$  structures. Such difference supports incorporation of two different RE atoms into the structure and, ultimately, its stability.

## ■ ASSOCIATED CONTENT

### 📄 Supporting Information

Magnetic measurements of the  $\text{Ce}_{1.5}\text{Ho}_{1.5}\text{SbO}_3$  sample are presented, as well as the calculated densities of states for the  $\text{RE}^{\text{I}}_{1.5}\text{RE}^{\text{II}}_{1.5}\text{SbO}_3$  phases adjusted to  $\text{RE}^{\text{I}}\text{RE}^{\text{II}}_2\text{SbO}_3$  stoichiometries via full occupation of the RE sites based on the site preferences derived from the X-ray single-crystal solutions. The crystallographic data for the  $\text{Dy}_3\text{SbO}_3$  phase as well as the other phases are presented. This material is available free of charge via the Internet at <http://pubs.acs.org>.

## ■ AUTHOR INFORMATION

### Corresponding Author

\*E-mail: [mozhar@mcmaster.ca](mailto:mozhar@mcmaster.ca).

### Notes

The authors declare no competing financial interest.

## ■ ACKNOWLEDGMENTS

This work was supported by a Discovery Grant from the Natural Sciences and Engineering Research Council of Canada.

## ■ REFERENCES

(1) Bell, L. E. *Science (Washington, DC, U. S.)* **2008**, *321* (5895), 1457–1461.

- (2) LaGrandeur, J.; Crane, D.; Hung, S.; Mazar, B.; Eder, A. *Int. Conf. Thermoelectr.* **2006**, *25th* (Pt. 1), 343–348.
- (3) Yang, J.; Caillat, T. *MRS Bull.* **2006**, *31* (3), 224–229.
- (4) Watanabe, S. *Manufacture of thermoelectric generator*. JP06338636A, 1994.
- (5) Rowe, D. M. *CRC Handbook of Thermoelectrics: Macro to Nano*; CRC: Boca Raton, 2005.
- (6) Slack, G. A. In *CRC Handbook of Thermoelectrics*; Rowe, D. M., Ed.; CRC Press: Boca Raton, FL, 1995.
- (7) Caillat, T.; Fleurial, J. P.; Borshchevsky, A. *J. Phys. Chem. Solids* **1997**, *58* (7), 1119–1125.
- (8) Mozharivskiy, Y.; Pecharsky, A. O.; Bud'ko, S.; Miller, G. J. *Chem. Mater.* **2004**, *16* (8), 1580–1589.
- (9) Snyder, G. J.; Christensen, M.; Nishibori, E.; Caillat, T.; Iversen, B. B. *Nat. Mater.* **2004**, *3* (7), 458–463.
- (10) Beyer, H.; Nurnus, J.; Bottner, H.; Lambrecht, A.; Roch, T.; Bauer, G. *Appl. Phys. Lett.* **2002**, *80* (7), 1216–1218.
- (11) Harman, T. C.; Spears, D. L.; Manfra, M. J. *J. Electron. Mater.* **1996**, *25* (7), 1121–1127.
- (12) Wang, P.; Forbes, S.; Kolodiazny, T.; Kosuda, K.; Mozharivskiy, Y. *J. Am. Chem. Soc.* **2010**, *132* (25), 8795–8803.
- (13) Wang, P. L.; Kolodiazny, T.; Yao, J.; Mozharivskiy, Y. *J. Am. Chem. Soc.* **2012**, *134* (3), 1426–1429.
- (14) *STOE X-Shape*; STOE & Cie GmbH: Darmstadt, Germany, 2004.
- (15) Sheldrick, G. M. *SHELXL*; University of Gottingen: Germany, 1997.
- (16) Hamilton, W. C. *Acta Crystallogr.* **1965**, *18* (3), 502–10.
- (17) Hunter, B. A.; Howard, C. J. *Rietica Australian Nuclear Science and Technology Organization*; Lucas Heights Research Laboratories: Menai, Australia, 2000.
- (18) Koch, E.; Fischer, W. Z. *Kristallogr.* **1996**, *211*, 251–253.
- (19) Andersen, O. K.; Pawlowska, Z.; Jepsen, O. *Phys. Rev. B: Condens. Matter Mater. Phys.* **1986**, *34*, 5253–69.
- (20) Jepsen, O.; Burkhardt, A.; Andersen, O. K. *The TB-LMTO-ASA Program*, version 4.7; Max-Planck-Institut für Festkörperforschung: Stuttgart, Germany, 1999.
- (21) Andersen, O. K.; Jepsen, O. *Phys. Rev. Lett.* **1984**, *53*, 2571–2574.
- (22) Andersen, O. K.; Jepsen, O.; Glotzel, D. In *Highlights of Condensed Matter Theory*; Bassani, F., Fumi, F., Tosi, M. P., Eds.; Elsevier: Amsterdam, 1985.
- (23) Jepsen, O.; Andersen, O. K. *Phys. Rev. B: Condens. Matter* **1995**, *97*, 35–47.
- (24) Shannon, R. D. *Acta Crystallogr., Sect. A* **1976**, *A32* (5), 751–67.
- (25) Papoian, G. A.; Hoffmann, R. *Angew. Chem., Int. Ed.* **2000**, *39* (14), 2409–2448.
- (26) Sootsman, J. R.; Chung, D. Y.; Kanatzidis, M. G. *Angew. Chem., Int. Ed.* **2009**, *48* (46), 8616–8639.